Modeling the Dynamics of Subducting Slabs

Magali I. Billen

Department of Geology, University of California, Davis, California 95616;
email: billen@geology.ucdavis.edu

Annu. Rev. Earth Planet. Sci. 2008. 36:325–56

First published online as a Review in Advance on February 12, 2008

The *Annual Review of Earth and Planetary Sciences* is online at earth.annualreviews.org

This article's doi:
10.1146/annurev.earth.36.031207.124129

0084-6597/08/0530-0325$20.00

Key Words

subduction, rheology, phase transition, mantle convection, numerical methods

Abstract

Cold, dense subducting lithosphere provides the primary force driving tectonic plates at Earth's surface. The force available to drive the plates depends on a balance between the buoyancy forces driving subduction and the mechanical and buoyancy forces resisting subduction. Because both the buoyancy and rheology of the slab and mantle depend on temperature, composition, grain size, water content, and melt fraction, unraveling which of these processes exert a first-order control on slab dynamics and under what circumstances other processes become first-order effects can be challenging. Laboratory and numerical models of slab dynamics provide a powerful method for testing the combined effects of buoyancy and strength changes that accompany the slab evolution in the upper mantle, transition zone, and lower mantle. Recent studies have focused on understanding how rheologic variations (Newtonian versus non-Newtonian viscosity or water content), geometry (2D versus 3D), and plate motions (trench roll-back or advance) influence the evolution of slabs in the upper mantle and how they sink into the lower mantle. These models suggest that spatial and temporal variations in slab strength and the history of subduction determine whether slabs sink directly into the lower mantle or are trapped in the transition zone.

INTRODUCTION

What is Subduction Dynamics?

Subduction: the term subduction was introduced into the literature in 1970 as an alternative to a large range of descriptive terms to describe the complete underthrusting of one plate beneath another

Slab: 3D section of subducted lithosphere in the mantle

The topic of subduction dynamics encompasses a tightly coupled system of geophysical, petrological, and geochemical processes. On the tectonic scale, the study of subduction dynamics focuses on the long-term evolution of slabs, and developing a physically consistent model capable of explaining the diverse morphology of slabs imaged in seismic tomographic studies (**Figure 1*a***; Lay 1994, Romanowicz 2003). At the regional scale, the focus turns to the effects of compositional layering, shallow phase transitions associated with dehydration of the slab, and hydration and melting in the mantle wedge (**Figure 1*b***; Poli & Schmidt 2002). When combined with experimental constraints on mineral physics and rheology, and a suite of observations ranging from the stress orientations in slabs to the geoid, geodynamical models of subduction provide a powerful tool for determining the properties of the subducted lithosphere and mantle and the dynamical processes that control slab evolution.

In recent years, the growth in the power of computing and advances in laboratory modeling techniques have supported the development of 2D and 3D models exploring a range of factors related to several outstanding questions of slab dynamics: How strong are slabs and how does their strength vary with depth and deformation? Is trench motion a cause or effect of slab dynamics? Why do some slabs appear to sink directly into the lower mantle, whereas others appear to be stranded in the transition zone? These questions have been at the core of subduction dynamics studies since the advent of plate tectonics, and their answers are ultimately related to how mantle convection drives plate tectonics on Earth.

Historical Perspective Framing Modern Investigations

The realization that cold oceanic crust and lithosphere sinks as coherent slabs into the mantle was one of the last developments in the theory of plate tectonics. Although Holmes (1944) described how thermal convection in the mantle could drive plate motion, the concept of complete underthrusting of the oceanic plate was not accepted until after the magnitude 9.2 Alaska 1964 earthquake. Surveying of surface uplift following this event required a large, shallowly-dipping thrust fault under the continent that reached the surface outboard of the continent (Plafker 1965). Prior to this observation, deep seismicity was interpreted to occur on a "mega-fault" extending from the surface to a depth of 700 km (Benioff 1954), and seafloor spreading was thought to be accommodated by crustal-scale thrusting (Hess 1962). Even in the seminal paper by Elsasser (1968) presenting a nearly modern view of how mantle convection drives plate tectonics, including the importance of stress- and water-dependent rheology, deep seismicity was still thought to occur on a planar boundary between the sinking lithosphere and surrounding mantle. Only with the development of regular determination of earthquake focal mechanisms for several of the world's zones of deep seismicity were intermediate and deep earthquakes properly understood as reflecting the internal deformation of sinking lithosphere (Isacks & Molnar 1969). The observation made at that time, that the strain-state in different regions of subducted

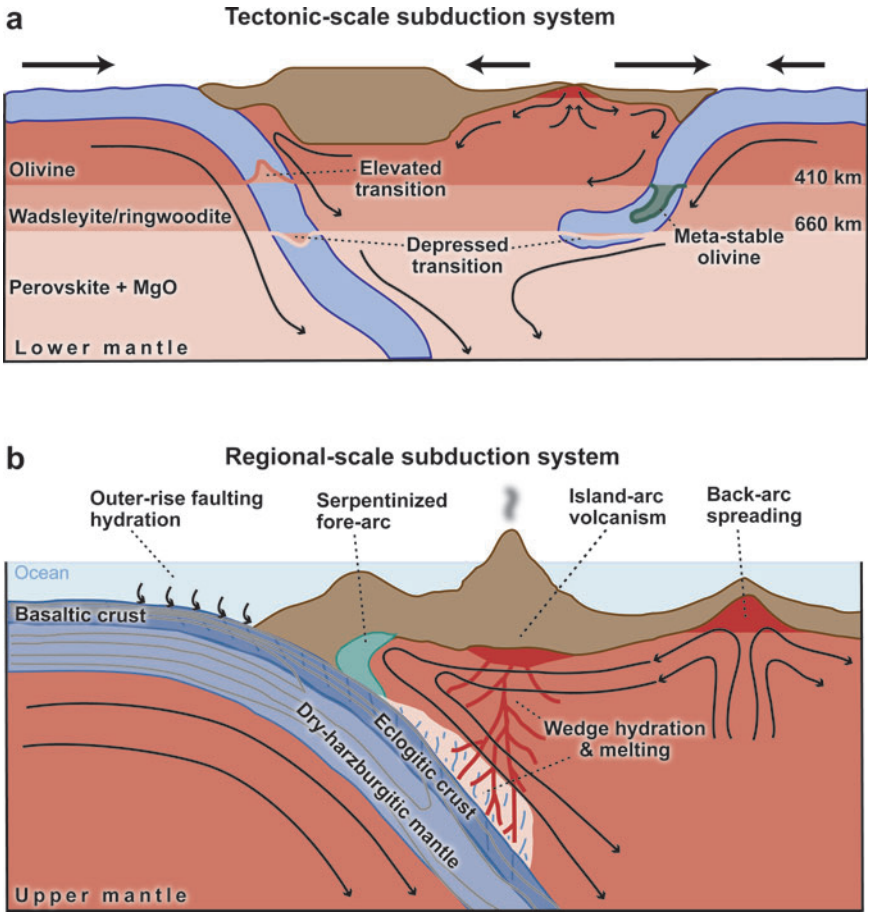

Figure 1

Tectonic- versus regional-scale processes in the subduction system. (*a*) On the tectonic scale, the subduction system is not likely to be steady-state and slab evolution depends on the character and geometry of overriding tectonic plates, layers of varying viscosity and density, other regions of upwelling or downwelling, and long-term history of mantle convection in addition to the slab density and rheology. (*b*) On the regional scale, details of the compositional and rheologic structure of the subducting and overriding plates and petrologic processes in the mantle wedge (melting, dehydration) affect the local balance of forces and thermal evolution of the subduction system.

lithosphere varies from dominantly down-dip compression to down-dip extension, continues to be enigmatic.

Although deep seismicity clearly pointed to internal deformation of slabs, the first quantitative studies of subduction dynamics used analytic models that approximated the highly viscous slab as a perfectly rigid plate sinking into the mantle at a fixed dip and rate (McKenzie 1969). This model predicted that subduction-induced flow in the mantle would take the form of a corner-flow, which creates a net upward suction

Dynamic models: simulations in which all three conservation equations are solved (mass, momentum, and energy); the thermal field, as well as the viscosity, composition, and phase changes, are updated for each time-step

force on the rigid slab. It was later shown that a steady-state balance between the buoyancy force causing the slab to sink and the flow-induced stresses pulling the slab up into the mantle wedge provided an accurate prediction of the average dip of slabs in the upper mantle (~50–60°; Stevenson & Turner 1977, Tovish et al. 1978). Although this agreement with observations attests to the ability of this simple model to capture the fundamental forces determining slab dynamics (buoyancy and viscous shear), the result depends on the assumption of a perfectly rigid slab that is free to pivot in response to the flow-induced stresses on its boundaries. However, such an assumption is only valid if the slab is strong enough to support its own weight and responds to flow-induced stresses without yielding.

The earliest numerical and laboratory models of slab deformation made the assumption that subducted lithosphere is only moderately (10–100×) more viscous than the surrounding mantle. One of the first purely viscous models of subduction predicted that slabs impinging on a higher viscosity lower mantle would be in down-dip compression to shallow depths (Vassiliou et al. 1984). Subsequently, it was also shown that the depth distribution of earthquake frequency is well predicted by strain-rate distribution in a moderately viscous slab (Tao & O'Connell 1993). In addition, the first time-dependent, dynamic model of subduction showed that a moderate increase in viscosity between the upper and lower mantle and a moderately viscous slab provided a good match to the average dip of slabs and observed shallowing of deep slab dip with subduction duration (Gurnis & Hager 1988).

These early studies set the stage for modern studies of slab dynamics. Today, as then, the fundamental questions concerning slab dynamics are (*a*) What is the net buoyancy available to drive subduction and how might it vary between subduction zones, and (*b*) What is the rheology of the slab and surrounding mantle. Because the processes affecting buoyancy (temperature, phase transitions, composition) also affect rheology, determining which processes actually affect slab dynamics requires systematic study, innovative techniques, and creative use of available observations.

BALANCE OF FORCES IN THE SUBDUCTION SYSTEM

The evolution of subducted slabs depends on the balance of driving and resisting forces, how these forces change with depth and time, and the geometry imposed by the larger-scale tectonic environment (**Figure 2**). Driving forces include ridge-push, the negative buoyancy owing to cold thermal anomalies and elevation of the olivine-to-wadsleyite (α-to-β olivine; spinel-structure) phase transition at a depth of 410 km. Resisting forces include bending of the lithosphere and frictional plate-coupling at shallow depths, viscous shear in the mantle, and positive buoyancy forces owing to the ringwoodite-to-perovskite plus magnesiowustite (spinel-to-perovskite + MgO) phase transition at a depth of 660 km and, possibly, a delayed transition of olivine to wadsleyite at 410 km (meta-stable olivine). In addition to the local forces, large-scale mantle flow and flow-induced pressure anomalies also affect the sinking rate and geometry of subducting lithosphere.

The relative importance of each of the driving and resisting forces depends on the details of the subduction history (e.g., age of the subducting lithosphere, plate

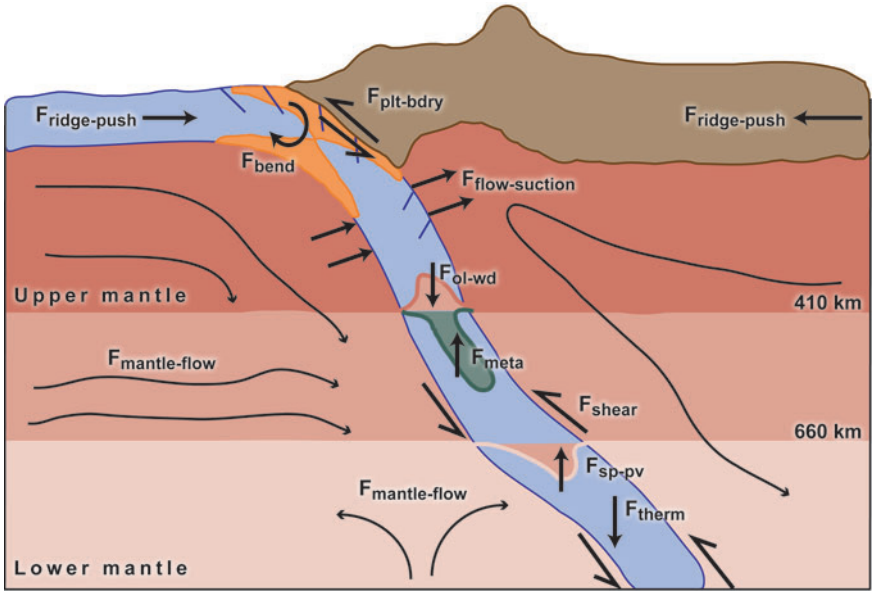

Figure 2

Schematic illustration of the forces acting on slabs. Driving forces include negative buoyancy (higher density) caused by cold thermal anomalies and an elevated phase change at 410 km within the slab. Resisting forces at shallow depth include bending of the plate in the trench and coupling to the overriding plate. In the upper mantle, subduction is resisted by viscous shear and positive buoyancy (lower density) owing to a depressed phase transition at 660 km and/or meta-stable olivine below 410 km. In the lower mantle, viscous shear increases. In addition, flow-induced suction in the mantle wedge and large-scale mantle flow affects the evolution of the slab.

boundary dip and mechanical properties, sinking rate, duration of subduction). However, examining the relative magnitude of these forces, and how they depend on a few key parameters, provides insight into which properties control slab dynamics and under what circumstances other properties become more or less important. For example, early subduction models assumed that deep earthquakes stopped at 660 km because slabs heated up rapidly and therefore the negative buoyancy of the slab was limited to the upper mantle [e.g., kinematic models of slab thermal evolution by Toksöv et al. (1971)]. However, the theory that deep earthquakes are thermally controlled has been superseded by other mechanisms that rely on a cold, and hence dense, slab (Green & Houston 1995). Therefore, the ability of slabs to subduct deep into the mantle depends on the magnitude of other buoyancy forces arising in the slab that either aid or hinder subduction and to the viscous shear forces opposing subduction.

Kinematic models: simulations in which the velocity for part of the interior of the model domain (e.g., the slab) is prescribed for all time-steps

Illustrative Example: Simplified Force-Balance on a Slab

To illustrate the balance of forces in the mantle, consider a slab sinking vertically into the mantle in which the thermal anomaly at any depth is Gaussian and the maximum

thermal anomaly decreases exponentially with depth,

$$\Delta T(x, z) = A(e^{-z/Bz_{slab}} - e^{-1/B})e^{-(x/w_{slab})^2}, \quad (1)$$

where $A = \Delta T_{\max}/(e^{-z_{\min}/Bz_{slab}} - e^{-1/B})$ scales the anomaly to have a maximum value of $\Delta T_{\max}$ at $x = 0$ and $z = z_{\min}$, B is a constant that controls the exponential decay of the thermal anomaly with depth, and w_{slab} is the half-width of the thermal anomaly (40 km). **Figure 3** shows the thermal anomaly for a cold slab ($\Delta T_{\max} = 1200^{\circ}$C, $B = 3.0$) extending to a depth of 1240 km and 840 km. In this simplified model, deeper slabs are colder slabs (i.e., there is no assumption of thermal steady-state).

The force available to drive subduction of the lithosphere can be expressed as the sum of driving and resisting forces,

$$F_{tot} = F_{therm} + F_{shear} + F_{sp-pv} + (F_{ol-wd}) + (F_{meta}), \quad (2)$$

where F_{therm} is the buoyancy force owing to the thermal anomaly of the slab, F_{shear} is the viscous shear force, F_{ol-wd} and F_{sp-pv} are the buoyancy forces owing to the upper mantle phase transitions, and F_{meta} is the buoyancy force owing to a metastable olivine wedge. In the force-balance calculations, only one of F_{ol-wd} or F_{meta} is included depending on whether the phase transition is assumed to be kinetically delayed. For this illustrative example, the effects of bending forces, plate boundary coupling, or large-scale mantle flow are ignored. In addition, the shear forces are simply modeled as resulting from a linear velocity gradient on the sides of the slab,

$$F_{shear} = \frac{2v_{slab}}{w_{slab}}(\eta_{um} z_{slab-um} + \eta_{lm} z_{slab-lm}). \quad (3)$$

The length of the slab is divided into upper and lower mantle portions, $z_{slab-um}$ and $z_{slab-lm}$, corresponding to a two-layer viscosity structure ($\eta_{um} = 10^{19}$ or 10^{20} Pa s; $\eta_{lm} = 10^{21}$ Pa s). Because the velocity is prescribed, when $F_{tot} = 0$ the forces are balanced for the given velocity, whereas for $F_{tot} > 0$ the forces are sufficient to drive subduction at a faster rate than prescribed, and for $F_{tot} < 0$ the resisting forces would slow down subduction.

The buoyancy forces associated with the phase transitions depend on both the clapeyron slope, γ, and the density change, $\Delta\rho$. The density change is 3.0%–5.7% for the olivine-wadsleyite transition and 7.0%–9.3% for the ringwoodite-perovskite transition (Dziewonski & Anderson 1981, Kennett et al. 1995, Weidner & Wang 1998). The clapeyron slope for the olivine-wadsleyite transition is $\gamma_{410} = 2.5$–4.0 MPa K^{-1} (Katsura & Ito 1989, Morishima et al. 1994, Katsura et al. 2004), whereas the magnitude of the clapeyron slope for the ringwoodite-perovskite transition has changed significantly from earlier experimental values of $\gamma_{660} \geq -6$ MPa/K to $\gamma_{660} = -0.5$ to -3.0 MPa/K for more recent experiments, which are better able to constrain the pressure of the phase transition at different temperatures (Ito & Takahashi 1989, Irifune et al. 1998, Katsura et al. 2003, Fei et al. 2004, Litasov et al. 2005). In the examples below we use $\Delta\rho_{410} = 3.0\%$, $\gamma_{410} = 4.0$ MPa K^{-1}, $\Delta\rho_{660} = 7.0\%$, $\gamma_{660} = -2.0$ MPa K^{-1}, unless otherwise noted.

Although the positive clapeyron slope for the olivine-wadsleyite transition creates a negative buoyancy anomaly that aids subduction, if this transition is kinetically

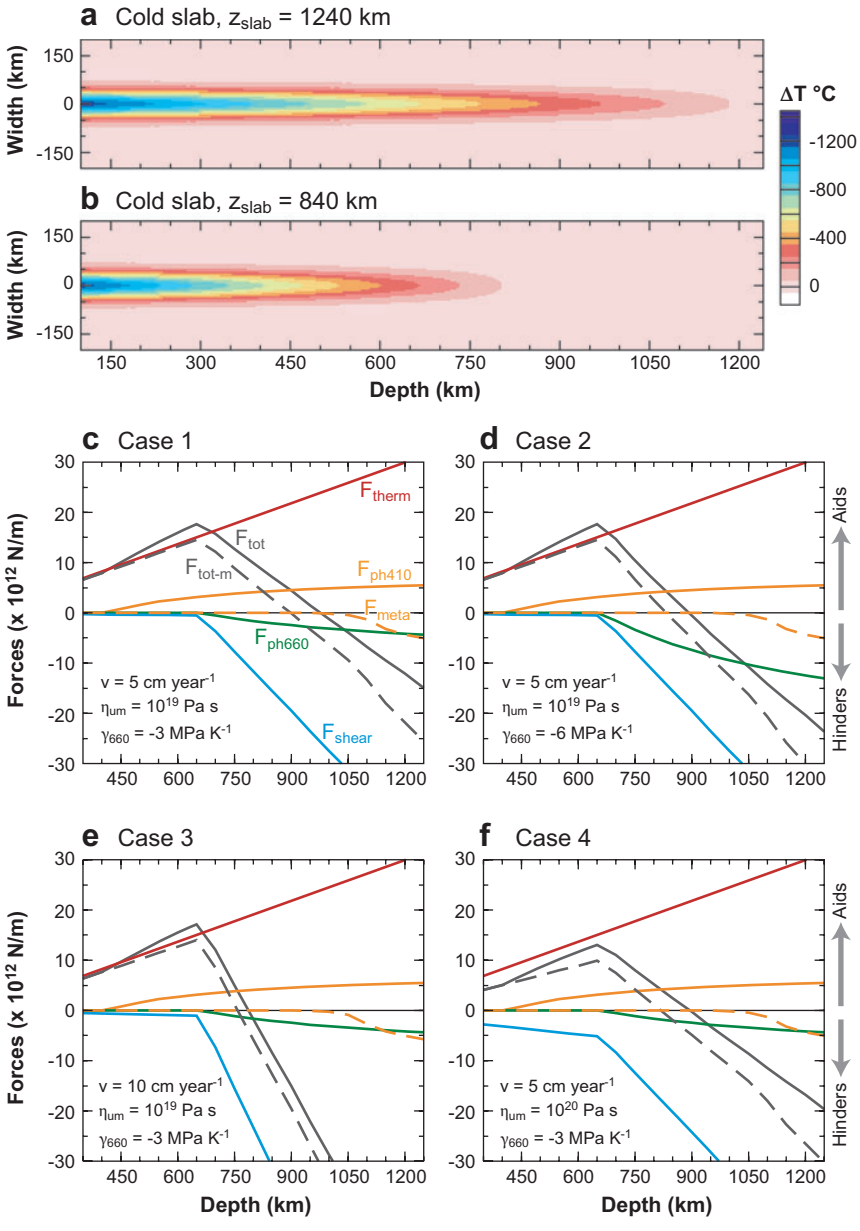

Figure 3

Simplified model of slab forces. (*a*) Thermal anomaly for a slab extending to 1240 km. (*b*) Thermal anomaly for a slab extending to 840 km. (*c–f*) Buoyancy and viscous shear forces for cases 1–4. Each curve is labeled in part (*c*): F_{tot-m} includes the positive buoyancy owing to meta-stable olivine, whereas F_{tot} includes the negative buoyancy owing to the olivine-wadsleyite transition. All parameters are given in the text except as noted in each figure panel.

delayed in cold, fast subducting slabs, then the meta-stable olivine wedge would contribute a positive buoyancy anomaly relative to the surrounding mantle (Kirby et al. 1991, Rubie & Ross 1994). The magnitude of this contribution can be estimated using an empirical model that accounts for the grain size, sinking velocity, and experimental constraints on the kinetics of the phase transition (for details of the model and parameters, see Mosenfelder et al. 2001).

Figures 3*c–f* show how each of the driving and resisting forces changes with the maximum depth of the slab, z_{slab}, where positive forces aid subduction and negative forces hinder subduction. Comparison of all the cases shows that the slab thermal buoyancy and the viscous shear forces in the higher viscosity lower mantle have the largest magnitudes. The maximum density anomaly associated with the thermal anomaly of the slab is ~80 kg m^{-3} or 2.4%, which is similar to the density anomaly associated with the olivine-wadsleyite phase change, but approximately half the density anomaly of the ringwoodite-perovskite transition. However, the full volume of the thermal anomaly contributes some proportion of this density anomaly to the slab buoyancy force and therefore the thermal buoyancy grows rapidly with the length of the slab. In case 1, with a slab velocity of 5 cm year^{-1} and $\eta_{um} = 10^{19}$ Pa s, the driving forces are larger than the resisting forces for a slab length up to 1000 km. Although the lower mantle shear forces have the biggest effect on the force-balance (case 1 versus case 3), a factor of 10 increase in the viscosity of the upper mantle decreases the slab length at which the forces are balanced by 150 km (case 1 versus case 4). This result suggests that the viscosity of the upper mantle, and whether it is treated as Newtonian or non-Newtonian (stress-dependent) in models, can have a significant effect on predicted slab evolution.

The buoyancy forces owing to the phase transitions and meta-stable olivine also shift the slab length at which the forces are balanced or prevent further sinking of the slab. For cases 1, 3, and 4, with $\gamma_{660} = -3$ MPa K^{-1}, the buoyancy force owing to the phase transitions shifts the depth at which $F_{tot} \leq 0$ by only 50 km because the effects of the two phase transitions roughly cancel. In contrast, for case 2 with a larger clapeyron slope of $\gamma_{660} = -6.0$ MPa K^{-1}, the positive buoyancy associated with the phase transitions shifts the depth at which $F_{tot} \leq 0$ to a slab length of only 900 km (**Figure 3*d***). Similarly, the positive buoyancy force owing to meta-stable olivine decreases the slab length at which forces are balanced by 50–100 km to a length of 800–900 km (dashed line in **Figure 3*c–f***). These results illustrate how important robust constraints on high-pressure mineral physics are to unraveling the processes affecting slab dynamics.

This force-balance model makes several simplifications about the magnitude of forces and how they are distributed in the subduction system, which can have important effects on the time-dependent evolution of slabs. While examining the net force-balance is illustrative, it implicitly assumes that the slab is capable of transferring stress from deep in the mantle to the shallow slab. However, the local balance of forces at different depths may instead lead to changes in geometry, such as shallowing, steepening, or buckling of the slab. In addition, the model specifies a subduction velocity to determine the shear forces, whereas in a self-consistent dynamic model, an increase in viscous resistance would decrease the slab velocity. In a dynamic model,

the slab may continue to sink in the lower mantle, although at a slower rate, or deform internally to accommodate the variations in viscous resistance. To address slab dynamics in Earth, numerical and laboratory simulations are used to test the effects of such non-steady-state behavior, 2D and 3D geometry of slabs, and more realistic rheology.

MODELING SUBDUCTION DYNAMICS

One of the main strengths of modeling subduction dynamics is the ability to test hypothesis regarding the effects of geometry, rheology, composition, melting, hydration, or phase changes. However, this strength is also an important weakness because every model result depends directly on which of these effects is incorporated and the values of the related parameters, which may or may not be well known. Therefore, although models of subduction dynamics are now capable of incorporating many of the complexities thought to occur in Earth, our understanding of the importance of these processes, how they interact, and the range of their effects is still in its infancy.

In most cases, long-term subduction dynamics is modeled using the viscous approximation, that is, over long times (greater than approximately 1 million years) the elastic response of the lithosphere and mantle can be ignored and only the viscous or visco-plastic behavior is considered. An important exception is subduction initiation (e.g., Toth & Gurnis 1998, Regenauer-Lieb et al. 2001, Hall et al. 2003). For viscous or visco-plastic rheology, the dynamics of the slab are determined by solving the standard equations of conservation of mass for an incompressible fluid,

$$\nabla \cdot \mathbf{u} = 0; \tag{4}$$

conservation of momentum for large Prandtl number flow (ignoring terms with factors of $1/Pr$ where, $Pr = \eta/\kappa\rho$) subject to the Boussinesq approximation (inertial forces are negligible so that density differences are ignored except when multiplied by g),

$$\nabla \cdot \sigma + \mathbf{f} = 0; \tag{5}$$

and the conservation of energy

$$\dot{T} = -\mathbf{u} \cdot \nabla T + \kappa \nabla^2 T + Q, \tag{6}$$

where $\mathbf{u}$ is the velocity, $\mathbf{f} = [\rho_o \alpha (T - T_o) + \Delta\rho_{pb} + \Delta\rho_c] g \delta_{rr}$ is the force owing to density variations related to temperature (T_o is a reference temperature), phase transitions ($\Delta\rho_{pb}$), and composition ($\Delta\rho_c$). The stress tensor defining the constitutive relation is $\sigma_{ij} = -P\delta_{ij} + \eta_{ef}\dot{\varepsilon}_{ij}$, where η_{ef} is the effective viscosity and the pressure, P, defined as the second invariant of the stress tensor, can be expressed as the sum of the lithostatic pressure, P_l (without compressibility), and the dynamic pressure, P_{dyn}, resulting from viscous flow (i.e., $P = P_l + P_{dyn}$). Internal heating, Q, is ignored in most studies of slab dynamics.

The challenge in solving these equations and the large variability in possible slab dynamics arises from the spatial variations in density and rheology owing to temperature, composition, and phase transitions. In addition, viscosity is stress dependent

(at least, in the upper mantle), which makes the momentum equation nonlinear in its dependence on velocity. Many of the recent studies in slab dynamics have focused on incorporating and understanding the role of these complexities in density and rheology structure.

Instantaneous models: simulations in which the equations of conservation of mass and momentum are solved, but not the conservation of energy; the thermal field is not advected forward in time

In the Laboratory or in a Computer?

Although the earliest understanding of slab dynamics came from analytic solutions (slab dip, plate bending), most studies of slab dynamics now involve either laboratory (analog) or numerical simulations. The choice of modeling technique depends on the specific question being addressed and/or the observations one seeks to understand. Early laboratory models were limited by the range in viscosity contrast provided by analog materials (only a factor of 10–500; Griffiths et al. 1995, Guillou-Frottier et al. 1995) and the inability to quantify aspects of the resulting flow (such as the velocity or strain rates). However, more recent models include viscosity variations of up to 4–5 orders of magnitude and use tracer bubbles with high-speed image capture processing, among other techniques, to quantify laboratory model results (Kincaid & Griffiths 2004, Funiciello et al. 2006). In addition, one of the important advantages of using laboratory experiments is the natural stress-free boundary on the top surface, which is more difficult to incorporate into numerical simulations. The main advantages of numerical simulations of slab dynamics is complete quantification of the flow field, inclusion of larger viscosity variations and stress-dependent viscosity, the size of the model domain (depth and horizontal extent), and potential to directly include the effects of melting or hydration/dehydration on density and viscosity. However, recent studies comparing laboratory and numerical simulations for identical model configurations show that both methods result in the same slab dynamics (Becker et al. 1999).

Different Model Types for Different Questions

Studies of subduction dynamics use a variety of model types or approaches that are best suited to explore different aspects of the subduction system or best exploit specific observations. These model types include instantaneous models and time-dependent models, which can range from fully dynamic to coupled kinematic-dynamic. In making the choice of model type and specifying the model setup, other general considerations include determining the appropriate domain size, addressing the effects (wanted or unwanted) of boundary conditions, what essential material properties need to be included, and the observations to which the model results are compared (**Table 1**).

Instantaneous models. At any instant in time the forces driving and resisting subduction must be balanced. This balance is expressed by the Navier-Stokes equation, which is simply the conservation of momentum (Equation 5) subject to conservation of mass (Equation 4). Using these equations, if the density and viscosity are prescribed everywhere in a model domain, and boundary conditions are defined, then the velocity field and pressure required to balance the forces can be found. From the velocity

Table 1 Summary of model types used to study subduction dynamics. Model design choices depend on the process being investigated and determine how boundary conditions may affect dynamics. Output parameters are a direct output of the model simulations, which can then be used to calculate other parameters to be compared with observations

Summary of Types of Subduction Models			
Model type	**Model design**	**Output parameters**	**Observations**
Instantaneous	Density and viscosity structure; model size; side, top, and bottom boundary conditions	Instantaneous velocity and pressure field	Dynamic topography, geoid, strain rate, stress orientations
Time-dependent			
Fully dynamic	Initial density, viscous, or visco-plastic flow law; model size; side, top, and bottom boundary conditions	Time-dependent velocity, pressure, temperature, composition, and density anomalies owing to phase changes	Same as instantaneous, plate rates and directions, uplift rates, time-dependent slab shape, correlation of slab geometry with other parameters
Dynamic with kinematic BC	Same as dynamic, prescribed plate motions at surface	Same as dynamic	Same as dynamic, except no uplift rates or dynamic topography
Coupled kinematic-dynamic	Slab geometry, subduction rate, thermal and viscosity structure of dynamic region, model size, boundary conditions	Steady-state velocity, pressure, and temperature	Heat flow, dynamic topography (upper plate), strain rates, accumulated strain

and pressure, surface plate motions, dynamic topography, the geoid, principal stress orientations, and the strain-rate field can also be determined. Instantaneous models of subduction dynamics are therefore used to understand how a density structure, perhaps inferred from seismic tomography, seismicity, or history of subduction, drives deformation given a specified viscosity structure.

Instantaneous models have been used to show that the observed geoid requires an increase in viscosity between the upper and lower mantle by 10–30 × (Hager 1984); that slabs with a moderately higher viscosity than the surrounding mantle (100–1000×) are needed to match the observed long-wavelength dynamic-topography high over subduction zones (Moresi & Gurnis 1996); that faulted plate boundaries provide good agreement with observed trench morphology (Zhong & Gurnis 1992, 1994); and that lateral variations in mantle viscosity structure, such as a low-viscosity region in the mantle wedge, can greatly diminish the magnitude of dynamic topography lows, switch the sign of the geoid, and switch the stress state from compressional to extensional in the overriding plate (**Figure 4**; Billen & Gurnis 2001, Billen et al. 2003).

The main advantage of using instantaneous models is that model results can be compared to a large range of present-day observations. The main disadvantage is that it is unknown whether the predefined density and viscosity structure adopted for the present geometry are consistent with the history of subduction.

Time-dependent models. By coupling the Navier-Stokes equation with the conservation of energy (Equation 6), the thermal structure evolves in time owing to

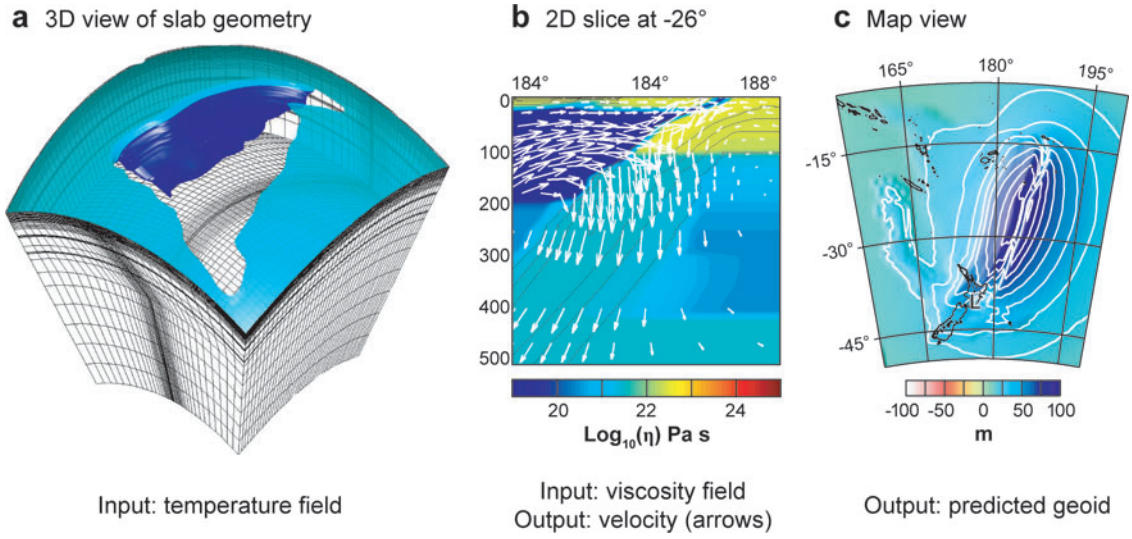

Figure 4

Example of a 3D instantaneous model of the Tonga-Kermadec subduction zone (Billen et al. 2003). (*a*) 3D view of Tonga-Kermadec slab thermal structure (input) inferred from seismicity, seismic tomography, and plate age. (*b*) 2D slice across 3D slab viscosity structure (input) showing the low viscosity wedge, and the instantaneous flow field (output). (*c*) Predicted geoid (output) showing the positive geoid anomaly over the subduction zone.

conduction and advection of heat and internal heat generation. Unlike instantaneous models, which use a prescribed slab structure, time-dependent models use a simple initial condition, such as the thermal model for a cooling plate, and an initial temperature or density perturbation to start subduction. The time-dependent evolution is then solved in three steps. First, the Navier-Stokes equation is solved for the initial condition (buoyancy and viscosity structure). Second, the velocity field is used in the conservation of energy equation to solve for a new temperature field. Third, any nonthermal sources of buoyancy are advected and a new viscosity structure is calculated for the new thermal/stress state. The process is then repeated for the new buoyancy and viscosity structure. Differences among time-dependent models depend on the type of boundary conditions used, model size and geometry, and the choice of material properties.

Dynamic models. Fully dynamic models of subduction have no prescribed velocity or applied force boundary conditions. In this case, the boundary conditions can be free-slip (also known as reflecting; stress tangential to the boundary and velocity perpendicular to the boundary are zero), stress free (also known as flow through; all stresses on the boundary are zero), or periodic (flow out of one side boundary reenters the box on the opposite side boundary). In fully dynamic models, only the buoyancy forces within the model domain can drive flow. However, many studies of slab dynamics use kinematic boundary conditions on the top surface to prescribe the

direction and rate of subduction and/or trench migration to explore how plate kinematics is related to the slab dynamics in the mantle (**Figure 5**; also see **Supplemental Movie 1**, follow the Supplemental Material link from the Annual Reviews home page at **http://www.annualreviews.org**). Implicit in the use of kinematic boundary conditions is the assumption that the boundary conditions do not create a flow that is inconsistent with the dynamic evolution of the slab. This assumption is valid for both moderately viscous slabs (Han & Gurnis 1999) and highly viscous slabs (Billen & Hirth 2007) with non-Newtonian viscosity.

In fully dynamic models and dynamic models with kinematic surface boundary conditions, the choice of side and bottom boundary conditions and model domain size does affect the pattern of flow and slab dynamics (**Figure 6**). For example, in 2D subduction models, the choice of periodic or flow-through side-wall boundary conditions imparts a net flow across the box, which may simulate large-scale mantle flow, whereas reflecting side-walls explicitly remove any net flow across the domain, allowing the local dynamics to be examined independently (Enns et al. 2005). However, the effect of boundary conditions also depends on the model domain size (**Figure 6**). For example, in a 2D model of subduction in a shallow box (i.e., maximum depth of 650–1500 km) with a low viscosity upper mantle and higher viscosity lower mantle, even if the side-walls are several box-depths away from the subducting slab (2500–6000 km), the return flow is focused in the upper mantle, creating a strong horizontal return flow that can cause even high-viscosity slabs to curl backward under the overriding plate (Billen & Hirth 2004). Increasing the box depth to the core-mantle boundary removes the strong lateral return flow in the upper mantle by allowing the flow to return through the deep lower mantle (Billen & Hirth 2007).

Dynamic models of subduction are generally used to investigate how slab evolution depends on various aspects of rheology and interaction with phase transitions. The model results can be compared to observed relations (e.g., Lallemand et al. 2005) between slab geometry or subduction history and other tectonic parameters, such as plate age, plate velocity, trench roll-back, or state of stress (e.g., Kincaid & Sacks 1997, Olbertz et al. 1997, Schmeling et al. 1999, Bellahsen et al. 2005, Stegman et al. 2006, Billen & Hirth 2007). In addition, models incorporating the history of plate motions for a specific region (as kinematic boundary conditions that change with time) can also compare the final model result with the present-day slab geometry to further constrain whether the modeled slab dynamics are consistent with observations (Tan et al. 2002).

Coupled kinematic-dynamic models. Large-scale models of subduction dynamics necessarily ignore many details of the flow and petrologic effects within the mantle wedge between the subducting slab and overriding plate owing to limitations on the model resolution and model size, and owing to the scientific questions being addressed. However, the local processes, such as melting, slab dehydration, and wedge hydration, and differences in behavior of different compositions affect both density and viscosity and therefore also influence how the slab couples to the mantle within the shallow subduction system. Mantle wedge dynamics are generally studied using coupled kinematic-dynamic models in which the velocity field of the entire slab is defined for all times, whereas the flow in the mantle wedge (and overriding plate) is

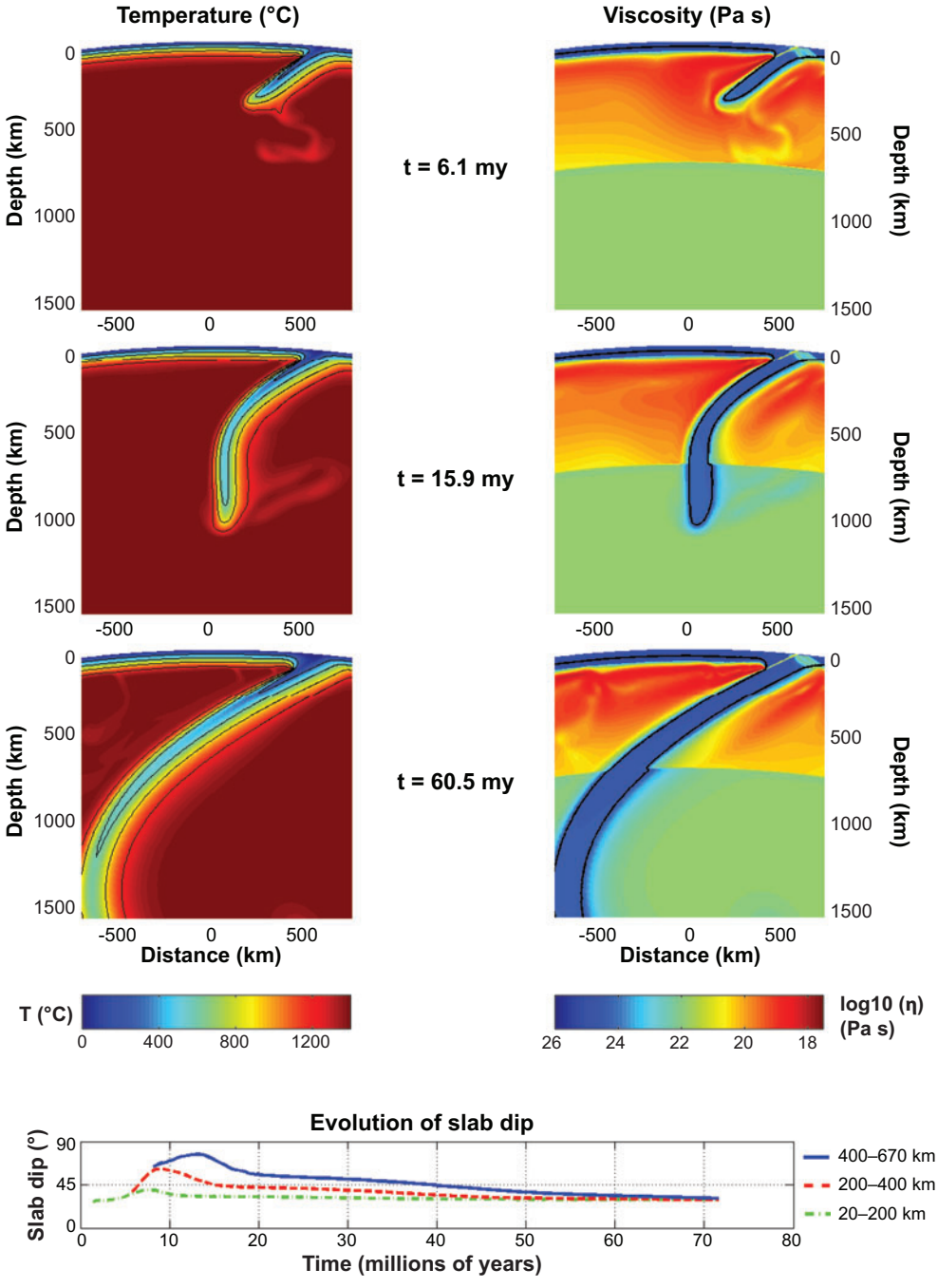

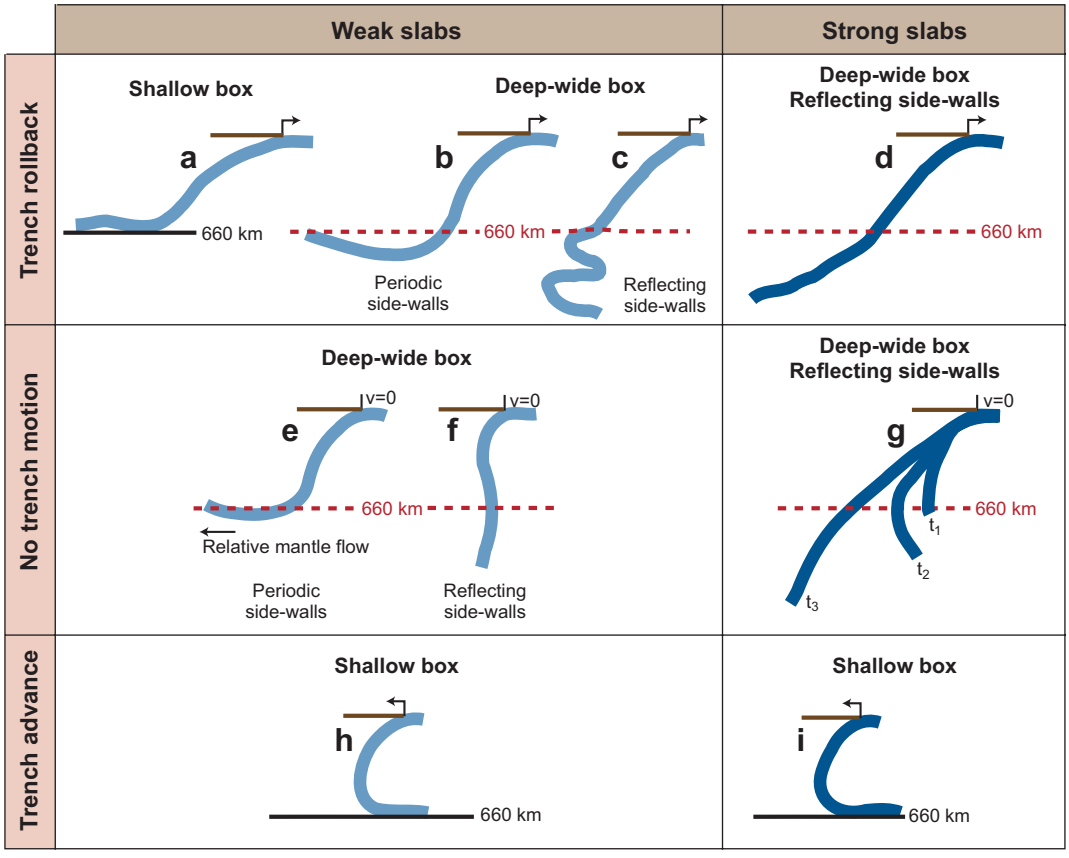

Figure 6

Slab morphology in laboratory and numerical models. Schematic illustration of the effects slab strength, trench motion, boundary conditions, and model domain size on slab dynamics from recent studies: (*a*) Funiciello et al. (2003), Schellart (2004), Bellahsen et al. (2005); (*b*) Han & Gurnis (1999); (*c*) Enns et al. (2005); (*d*) Cížková et al. (2002); (*e*) Enns et al. (2005); (*f*) Han & Gurnis (1999); (*g*) Billen & Hirth (2007); (*h*) Bellahsen et al. (2005); (*i*) Faccenna et al. (2007). Black line at 660 km depth indicates bottom boundary of model domain. Red dashed line at 660 km depth indicates change in viscosity and/or density structure (see original studies for details).

Figure 5

Example of 2D dynamic model of subduction with kinematic surface boundary conditions (Billen & Hirth 2007, see also **Supplemental Movie 1**). The subducting plate is moving at 10 cm year^{-1}. Only the subduction zone region is shown: the full model domain is 9100 km × 2890 km. Right: thermal structure. Left: viscosity structure. Bottom: shallow, intermediate, and deep slab dip as a function of time.

solved as a dynamic model with kinematic boundary conditions. The conservation of energy equation (thermal structure) is solved for the entire model domain and the model is typically run to steady-state (until the thermal structure does not change appreciably between time-steps). Such wedge dynamics models have been used to explore how mantle rheology affects thermal structure of the slab and overriding plate (Bodri & Bodri 1978, Furukawa 1993, Eberle et al. 2002, van Keken et al. 2002, Honda & Saito 2003, Kneller et al. 2007), fluid migration in the wedge (Cagnioncle et al. 2007), and deformation of the overriding plate (Gerya & Yuen 2003). However, because such models prescribed the geometry and velocity of the slab they can not be used to study slab dynamics directly and therefore are not discussed further.

PROCESSES AFFECTING SLAB EVOLUTION

An early model of mantle flow showed that the upper mantle dip of slabs is predicted by purely kinematically driven flow models (imposed surface plate motions) without internal variations in buoyancy or viscosity (Hager & O'Connell 1978). At first, this result seems to imply that slabs must respond passively to the large-scale mantle flow. However, if slabs are denser than the surrounding mantle, but weak, then they will sink vertically (King 2001), perturbing the kinematically driven flow pattern. Alternatively, the agreement between slab dip and the kinematically driven flow model may suggest that slabs (in the upper mantle) are strong enough to maintain shallow dips despite their negative buoyancy. Recent studies have focused on this long-lasting paradox in slab dynamics by exploring a variety of mechanisms affecting slab buoyancy, slab and mantle rheology, and the effects of large-scale mantle flow. These studies suggest that the strength of any particular slab may vary by several orders of magnitude along its length and that the history-dependence of subduction may determine when certain mechanisms (e.g., meta-stable olivine) exert first-order control on slab dynamics.

Slab and Mantle Rheology

The strength of the slab relative to the surrounding mantle depends on the dominate deformation mechanism (brittle, viscous, plastic yielding), which primarily depends on temperature and stress or strain rate (**Figure 7**). For example, the viscous deformation of olivine is described by an experimentally determined flow law,

$$\eta_{df,ds} = \left(\frac{d^p}{AC_{OH}^r} \exp(-\alpha\phi) \right)^{\frac{1}{n}} \dot{\varepsilon}_{II}^{\frac{1-n}{n}} \exp\left[\frac{E + P_l V}{nRT_c} \right] \tag{7}$$

(from Hirth & Kohlstedt 2003), where *df* and *ds* refer to deformation by diffusion creep ($n = 1$, Newtonian or linear viscosity) or dislocation creep ($n \approx 3.5$, non-Newtonian or nonlinear viscosity), respectively; E is the activation energy; V is the activation volume; $\dot{\varepsilon}_{II}$ is the second invariant of the strain-rate tensor; P_l is the lithostatic pressure, including a compressibility gradient in the mantle; and T_c is the temperature, including the adiabatic temperature gradient. In addition, the viscosity depends on the average grain size, d, the water content of the mineral phase, C_{OH} and the melt fraction, ϕ. It has long been known that owing to the large activation energy

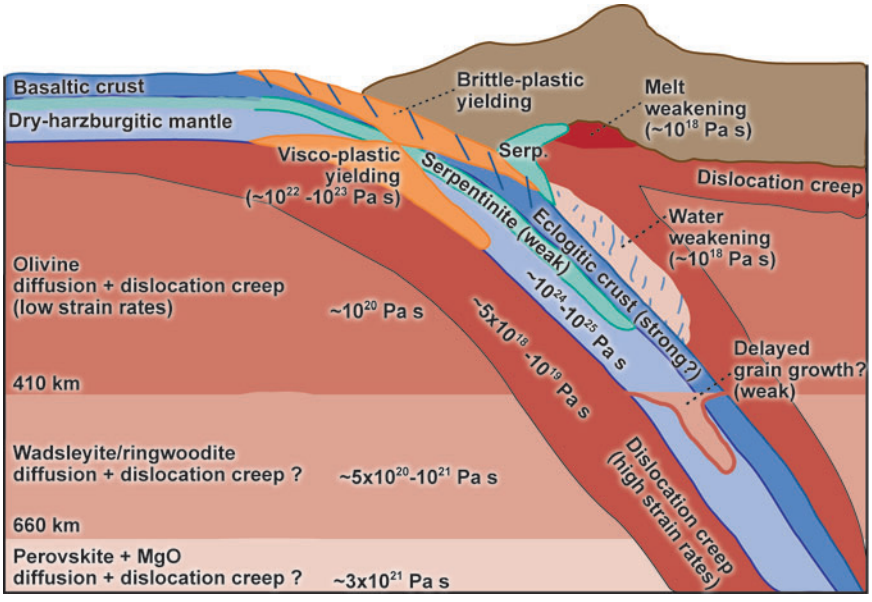

Figure 7

Rheology of the slab and mantle. Schematic showing variations in deformation mechanisms and processes affecting slab and mantle rheology: diffusion creep, dislocation creep, brittle and plastic yielding, grain-size reduction, phase change boundaries, temperature, water content, melt fraction and composition.

for diffusion creep in olivine, the cold interior of the slab should have a high viscosity compared with the surrounding mantle. In particular, at strain rates of 10^{-15} s^{-1} within the slab (Bevis 1988, Nothard et al. 1996), the viscous strength would exceed the theoretical yield strength of rock ($\sigma_y \geq 10$ GPa). Therefore, the upper bound on slab strength depends not on the viscous deformation, but on the yield (plastic) strength, which is estimated to be 300–1000 MPa (Goetze & Evans 1979, Evans et al. 1990). This range in plastic yield strength is roughly equivalent to an effective viscosity $\eta_{ef} = \sigma_y / \dot{\varepsilon}_{II}$ of greater than 3×10^{23} Pa s for strain rates less than 10^{-15} s^{-1} in the slab.

In the warm mantle, diffusion and dislocation creep mechanisms act together to accommodate deformation (composite viscosity). However, diffusion creep dominates deformation at cooler temperatures and larger grain sizes, whereas dislocation creep dominates deformation at higher strain rates and is not grain-size dependent. Experimental constraints are currently only available for deformation behavior of olivine and pyroxenes as upper mantle phases, so that the viscous behavior of the mantle deeper than 410 km is commonly assumed to be the same as olivine. In addition, seismic observations, which detect less seismic anisotropy in the lower mantle, suggest the lower mantle may deform primarily by diffusion creep (Savage 1999, Mainprice et al. 2005). New techniques are currently being implemented to facilitate deformation experiments at the pressures and temperatures appropriate for the transition zone (wadsleyite) and lower mantle (perovskite) phases (Cordier et al. 2004).

Slab strength and mantle rheology. As experimental constraints on the flow laws for olivine have improved, some models of slab dynamics have incorporated composite rheologies accounting for the diffusion and dislocation creep mechanisms and plastic yielding at high stress (**Figure 7**). Direct application of experimental flow laws in slab dynamics models leads to much stiffer slabs, up to 5–7 orders of magnitude more viscous than the surrounding mantle (Schmeling et al. 1999, Cížková et al. 2002, Billen & Hirth 2007), and a reduction in viscous shear stress on the slab in the upper mantle owing to the dislocation creep response to high strain rates surrounding the slab (Schmeling et al. 1999; Cížková et al. 2002; Billen & Hirth 2005, 2007).

For example, Cížková et al. (2002) show that stiffer slabs have shallower upper mantle dips and are more difficult to trap in the transition zone even when trench rollback rates exceed 4 cm year^{-1}. If trench motion is prevented, stiff slabs shallow with time beneath the overriding plate (Billen & Hirth 2007). This lateral migration occurs because it is easier for the slab to migrate laterally to accommodate the difference in sinking rates between the lower viscosity upper mantle and higher, Newtonian-viscosity lower mantle. Also, the observed correlation between subduction rate and trench motion rate is best fit with strong slabs (Faccenna et al. 2007). The way in which stiffer slabs accommodate changes in the resistance to sinking, however, also depends on the relative mantle flow. Models with relative motion between the slab and lower mantle tend to result in flat slabs in the upper-most lower mantle, whereas models without relative motion tend to develop slabs that buckle and fold (**Figure 6**; Enns et al. 2005, Stegman et al. 2006).

Because higher mesh resolution is required to accurately solve models with large viscosity variations, some models still use a viscosity cut-off value, which uniformly limits the maximum viscosity of the cold slab interiors (Han & Gurnis 1999, van Hunen et al. 2001, King 2001). However, limiting the viscosity with a yield stress leads to variations in the maximum viscosity of slabs in regions of large deformation and a very different behavior of slabs (Schmeling et al. 1999, Cížková et al. 2002, Enns et al. 2005, Stegman et al. 2006, Schellart et al. 2007, Billen & Hirth 2007). In particular, models with a viscosity cut-off tend to produce "taffy-like" slabs that sink vertically through the upper mantle and shorten to accommodate increased viscous resistance in the lower mantle (Han & Gurnis 1999, King 2001).

The combination of a yield stress and composite mantle viscosity in numerical models produces initially strong slabs that develop localized weak zones as the slab length increases. If the yield stress is moderate (500 MPa), slabs start off vertical, but their geometry may change as they interact with the lower mantle and stronger regions continue to transmit stresses up dip (Cížková et al. 2002, Billen & Hirth 2007). However, if the yield stress is low (<300 MPa), localized weakening can lead to slab break off for slabs as short as 300 km (Billen & Hirth 2007). Note, that the yield stress at which slab break off occurs depends on the mantle rheology. If the mantle viscosity is Newtonian, then more of the slab negative buoyancy is supported by viscous shear stresses and slab break-off may not occur (Enns et al. 2005, Stegman et al. 2006, Schellart et al. 2007).

Slab strength and trench motion. Seismicity and seismic tomography show that slabs exhibit a range of morphologies, from slabs trapped in the transition zone to slabs that appear to sink unhindered into the lower mantle (**Figure 1*a***). This variety in slab morphology and the lack of a dominant correlation between slab shape and other subduction parameters (e.g., slab buoyancy, roll-back rate) suggests that a combination of factors controls the evolution of slabs. On the top of the list of possibilities are processes that affect the strength of slabs, such as yielding and grain size reduction, and relative motion of the slab and surrounding mantle (roll-back or advance).

The role of trench motion as either a cause or effect of slab dynamics is not always clear, and the observations of absolute trench motion depend on the chosen reference frame (Garfunkel et al. 1986, Lallemand et al. 2005, Sdrolia & Müller 2006). However, laboratory and numerical models show that if slabs are prevented from subducting into the lower mantle, transmission of stresses along the slab to the overriding plate may cause trench motion (advancing or retreating) (Schellart 2004, Bellahsen et al. 2005), or if trench motion is imposed a priori, then slabs can be trapped in the transition zone (Cížková et al. 2002, Enns et al. 2005). Others have argued that changes in slab strength during subduction ultimately control whether stresses are transmitted up dip and therefore can affect trench motion (Karato et al. 2001, Faccenna et al. 2007).

A compilation of study results as a function of trench roll-back rate and maximum slab viscosity (**Figure 8**) shows that these two parameters can be used to separate modeled slabs into those that are trapped in the transition zone (for varying amounts of times) and those that subduct unhindered into the lower mantle (Zhong & Gurnis 1995, Christensen 1996, Olbertz et al. 1997, Han & Gurnis 1999, Tetzlaff

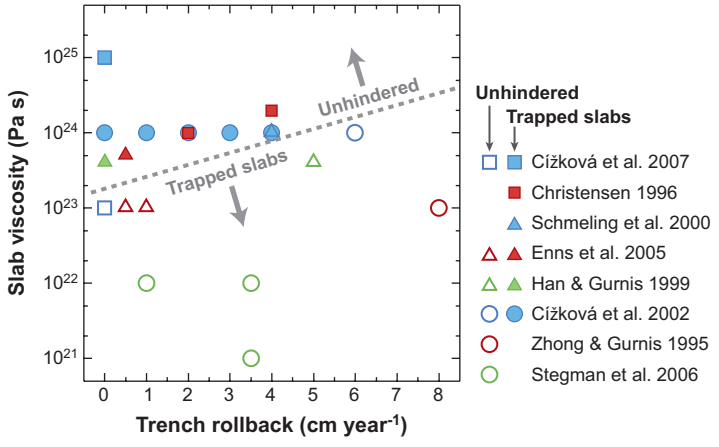

Figure 8

Conditions for trapping slabs in the transition zone. Summary of results for models of slab dynamics as a function of trench motion rate (centimeters per year) and maximum slab viscosity. Note that other parameters in the models may vary significantly between studies. Intermediate-to-fast trench roll-back and weaker slabs leads to trapped or delayed subduction. Open symbols: slabs penetrate into the lower mantle unperturbed. Closed symbols: trapped or delayed slabs.

& Schmeling 2000, Cížková et al. 2002, Enns et al. 2005, Stegman et al. 2006, Cížková et al. 2007). These models include the phase transitions at 410 and 660 km and an increase in viscosity of 10–100 between the upper and lower mantle. Slabs with strengths less than approximately 10^{23} Pa s (relative to an average upper mantle viscosity of 10^{20} Pa s) are trapped, regardless of the rate of trench roll-back, whereas slabs with viscosity greater than 10^{23} Pa s may be trapped for higher trench roll-back rates, but subduct unhindered for lower trench roll-back rates. Although each of these studies differs in the details of the model parameters, the results suggest that to obtain the range in slab morphology observed in Earth, the average viscosity of slabs must be greater than 10^{23} Pa s.

The minimum slab viscosity predicted from time-dependent models is greater than the typical values predicted by instantaneous models of present day subduction zones, which find that the long wavelength geoid (Hager 1984, Zhong & Davies 1999) and regional geoid and dynamic topography (Moresi et al. 1996, Billen & Gurnis 2001, Billen et al. 2003) are best fit with a slab viscosity less than 10^{22} Pa s. An important difference between these instantaneous models and the time-dependent models is the use of a yield stress. Whereas the instantaneous models use a viscosity cut-off and therefore a slab with a uniform maximum viscosity, the use of a yield stress leads to variations in viscosity along the slab. Therefore, the instantaneous models may be most sensitive to the weakest regions of the slab, such as the shallow hinge zone (**Figure 7**). However, this discrepancy in maximum slab viscosity has not yet been tested directly.

Secondary Rheologic Effects

Although the temperature and stress dependence of viscosity are the most important factors controlling slab strength in the upper mantle, other variations, such as water content, grain size, and composition, can also play an important role. These are globally secondary effects, but locally they can lead to variations in viscosity by 10^3–10^6 Pa s.

Water. The concentration of water in nominally anhydrous minerals (i.e., olivine) can vary from less than 10 ppm-H/Si to more than 3000 ppm-H/Si, which leads to a similar change in viscosity (Equation 7, $r = 1.0$–1.2). This effect probably plays a primary role in reducing the viscosity of the mantle wedge, which experiences an influx of water from the dehydrating slab, and in increasing the viscosity of the lithospheric-mantle portion of the plate, which is dehydrated during melting at the ridge (Braun et al. 2000). In instantaneous models, the presence of a low-viscosity wedge owing to water (and/or melt) decreases coupling between the subducting slab, mantle wedge, and overriding plate, increases the shallow depth extent of down-dip compression in slabs and leads to better predictions of the dynamic topography and short-to-intermediate wavelength geoid over subduction zones (Billen & Gurnis 2001, Billen et al. 2003, Billen & Gurnis 2003). In time-dependent models, an imposed wet, and therefore weak, wedge corner counteracts the increase in viscosity owing to cooling of the wedge nose (Kincaid & Sacks 1997) and maintains the

separation of the subducting and overriding plate (Cížková et al. 2007). In models where the low viscosity region develops over time in response to dehydration of the slab, the reduction in viscosity leads to small-scale convection that partially erodes the overriding plate in the subarc mantle (Arcay et al. 2005, 2006). This mechanism may play an important role in dynamically maintaining a thin lithosphere beneath the arc and allowing hot mantle to upwell to shallow depths above the slab.

A dry lithospheric-mantle changes the integrated strength of the slab by partially controlling the temperature at which deformation transitions from yielding in the cold interior of the slab to dislocation creep in the warmer, higher strain rate exterior of the slab. The larger integrated strength helps to support the negative buoyancy of the slab and decreases the average dip of modeled slabs by 15–30° (Billen & Hirth 2007).

Grain size. The effect of grain size on viscosity enters through the power-law dependence of diffusion creep on the average grain size (Equation 7, $p = 3$). Neither the average grain size or the variation in grain size in the mantle is well known. Xenoliths from the upper mantle typically have grain sizes of fractions of a millimeter to less than a centimeter (e.g., Titus et al. 2007). The presence of minor phases, such as pyroxenes, is thought to pin olivine grain growth, whereas recrystallization and dislocation creep also reduce grain size. One possibility is that in most regions of the mantle, the processes of grain growth and reduction are balanced and maintain grain-sizes on the order of a few millimeters (Hirth 2003, Hirth & Kohlstedt 2003). An important exception to this equilibrium grain-size model is grain growth following phase transitions in the cold interior of slabs. In the warm regions of the mantle, grain growth following a phase transition is rapid. However, in cold regions, grain growth may be kinetically delayed leading to isolated regions with small grain size and therefore lower viscosity than would be predicted based on temperature alone (Rubie 1984, Riedel & Karato 1997, Yamazaki et al. 2005).

Because diffusion creep viscosity is proportional to the cube of the grain size, a local reduction the grain size from 10 mm to 100 microns (factor of 100), is equivalent to a reduction in viscosity by 10^6, roughly negating the effects of temperature (Karato et al. 2001). However, the effect of a localized low-viscosity region in the slab following the olivine-wadsleyite phase transition at 410 km has been shown to have only a minor influence on slab dynamics in 2D because the stiff region surrounding the weak slab core continues to transmit stresses to the shallower portion of the slab (Cížková et al. 2002). The effect of grain size may still be an important factor in determining the strength of the slab in the lower mantle following the ringwoodite-perovskite transition at 660 km, which is accompanied by the cessation in deep seismicity (Karato et al. 2001).

Composition. The composition of the slab is also expected to lead to variations in the viscosity, which can also affect slab dynamics. For example, at shallow depths, basaltic crust may be weaker than the underlying harzburgitic mantle. However, once basalt transitions to eclogite (at a depth of ~50 km) which is rich in garnet, the crustal layer may in fact be stronger (Ji & Zhao 1994). Recent seismic observations also strengthen the evidence for serpentinization of the lithospheric-mantle beneath the crust in the

slab (Ranero et al. 2003), which could develop into a decoupling layer between the crust and deeper portions of the slab (Lee & Chen 2007). As with other factors, these compositional variations modify the integrated strength of the slab, which affects the way stress is transmitted up the slab from deeper in the mantle. These effects have not yet been directly incorporated into recent numerical models, so it is not known how they affect slab dip or the interaction of the slab with the phase transitions. However, previous models have shown that the downwelling flow induced by the sinking slab tends to keep the crust-lithosphere package together until the slab warms (i.e., weakens) in the lower mantle (Richards & Davies 1989, Xie & Tackley 2004).

Buoyancy forces. As illustrated with the simple force-balance calculation (**Figure 3**), the thermal buoyancy of a slab greatly exceeds other buoyancy forces owing to the large volume of the temperature anomaly as compared to the localized regions affected by phase transitions. However, the prediction that buoyancy forces owing to phase transition play a minor role is only true if the driving force of the thermal buoyancy is transmitted along the length of the slab, whereas variations in slab strength, as discussed above, can hinder the ability of the slab to act as a stress guide. In particular, if other processes, such as mantle flow or the motions of other plates decrease the slab dip in the transition zone, then positive buoyancy forces associated with phase transitions can have a first-order effect on slab dynamics.

For the ringwoodite-perovskite phase transition to affect the slab dynamics, the slab must actually cross a depth of 660 km (the phase transition is depressed to deeper depths creating the local density anomaly). Therefore, flat slabs should appear to lay partially below the transition zone in the upper-most lower mantle (Christensen 1996, Cížková et al. 2002). In contrast, if meta-stable olivine is the source of positive buoyancy, then slabs should appear trapped within the transition zone above 660 km (Schmeling et al. 1999, Tetzlaff & Schmeling 2000). The seismic observations interpreted as indicating significant volumes of meta-stable olivine in subducting slabs remain controversial. Meta-stable olivine is proposed to occur owing to slow kinetics in fast-subducting, cold slabs (Kirby et al. 1991, Rubie & Ross II 1994). However, the best evidence for meta-stable olivine does not occur in the coldest, fastest-subducting slab below the active Tonga-Kermadec subduction zone, but in a possible remnant slab of unknown age to the west below Fiji (Brudzinski & Chen 2000, Chen & Brudzinski 2001). In addition, the volume of meta-stable olivine is strongly dependent on the kinetic model for the phase transition (Rubie & Ross II 1994, Däbler & Yuen 1996, Mosenfelder et al. 2001), and the presence of water reduces the range of favorable temperatures from up to 1200°C to less than 600°C (Nishihara et al. 2006). Therefore, although meta-stable olivine could have an important influence on slab dynamics, the conditions under which dynamically significant volumes persist within slabs is still unknown.

3D Slab Dynamics

The community of geodynamicists using laboratory experiments has lead the study of time-dependent slab dynamics in three dimensions, and demonstrated some of the

important effects of trench motion and toroidal flow around the edges of slabs. These experiments have shown that resistance to subduction of the slab at depth can lead to either advancing or retreating motion of the trench depending on small initial perturbations in slab dip (Bellahsen et al. 2005, Schellart 2005). More importantly, flow of material around the edges of slabs causes slabs to develop convex trench-parallel profiles and the trench-parallel width of slabs affects the rate of trench motion (Schellart 2004, Funiciello et al. 2006). One limitation of laboratory models is the shallow depth extent of the models (670 km), which isolates slab-induced flow in the upper mantle and may accentuate the toroidal flow component. However, numerical models with a larger depth extent (1200 km) and a factor of 100 viscosity increase between the upper and lower mantle exhibit similar behavior (Stegman et al. 2006). The trench-parallel slab width also affects the morphology of slabs (Schellart et al. 2007): Narrow slabs (600 km) have rapid retreat rates and form concave profiles, whereas slabs with intermediate widths (2000 km) tend to be stationary and straight. However, the longest slabs show a mixed mode of deformation with stationary and straight central portions flanked by fast retreating and concave edges. This new explanation for the shape of trenches at the surface and the complex morphology of slabs suggests that overriding plate structure must play a minor role in determining plate boundary coupling and is instead dragged along by slab-induced flow.

STAGES OF SUBDUCTION

The evolution of slabs in the mantle can be divided into three stages: subduction initiation, long-term behavior, and subduction cessation. The models discussed thus far are focused on determining what controls the long-term evolution of slabs. These models show that many factors can affect slab dynamics and that slab evolution is inherently non-steady-state. Studies of subduction initiation or cessation are commonly treated separately from the long-term behavior of slabs. However, in addition to being complex and enigmatic processes, these special stages of slab evolution can provide important constraints on parameters affecting the long-term behavior of slab dynamics and clues into the unique occurrence of plate tectonics on Earth.

Subduction Initiation

The feasibility of subduction initiation has been studied using analytic models (McKenzie 1977, Cloetingh et al. 1989, Mueller & Phillips 1991, Fowler 1993, Kemp & Stevenson 1996, Niu et al. 2003) and numerical models addressing various weakening mechanisms or driving forces (Toth & Gurnis 1998, Regenauer-Lieb et al. 2001, Doin & Henry 2001). Recent numerical models have shown that ridge-push forces are sufficient to overcome the resisting forces of a visco-plastic plate if there is a preexisting weak zone, such as fracture zone, and subduction becomes self-sustaining when the slab length reaches approximately 100–150 km (Hall et al. 2003, Gurnis et al. 2004). These models use a composite viscosity similar to that used in long-term slab evolution models with strong slabs (Cížková et al. 2002, Billen & Hirth 2007). Therefore, uniformly weak slabs are also not needed to explain subduction initiation.

In addition, non-Newtonian rheology may be required to reduce viscous coupling between the nascent slab and overriding plate (Billen & Hirth 2005), although water or melt weakening could have a similar effect.

Cessation of Subduction

There are several processes that can lead to the demise of an active subduction zone: collision of a large oceanic plateau or continent, subduction of a ridge or transform fault, or major plate reorganization (Zeck 1996, Wong A Ton & Wortel et al. 1997, Ferrari 2004). Lithosphere subducted just prior to cessation of subduction may remain attached to the surface plate, slowly thermally reequilibrating with the surrounding mantle (van Wijk et al. 2001), or the driving forces of the deeper slab may cause the slab to break off from the surface plate. The conditions under which slab break off may occur have been addressed in several feasibility studies, which showed that slab strength is the main unknown parameter (Yoshioka et al. 1994, Davies & von Blanckenburg 1995, Wortel & Spakman 2000, Li et al. 2002). Subsequently, 2D time-dependent models have shown slab break off can only occur for very strong slabs (yield stress greater than 10 GPa) if shear heating or melting occur (Gerya et al. 2004). However, for a yield stress 300–500 MPa, break off occurs along a narrow shear zone in less than a few million years (Andrews & Billen 2008). These studies also illustrate the importance of mantle rheology. In models with a Newtonian (diffusion creep) upper mantle, slab break off does not occur, and instead slabs heat up for more than 100 million years before weakening sufficiently to drip into the mantle.

SUMMARY POINTS

1. Slab dynamics is controlled by a balance between driving and resisting forces, which can vary with depth, subduction rate, and the long-term evolution of the slab.
2. Although the thermal buoyancy of slabs in the upper mantle far exceeds the viscous shear resistance, the combined effects of other positive buoyancy forces, weakening of the slab, and changes in slab geometry can trap the slab in the transition zone.
3. Maximum slab viscosity is determined by the plastic yield strength, whereas the integrated strength depends on temperature and variations in water content, grain size, and composition.
4. 3D time-dependent models demonstrate that toroidal flow around the edges of slabs has first-order effects on slab dynamics.

FUTURE ISSUES

1. Although the importance of slab strength and mantle viscosity and density structure has been demonstrated in 2D models, integration of these

processes into 3D models is needed to understand how the local balance in forces affects the 3D geometry and evolution of slabs.

2. Systematic incorporation and testing of the effects of other buoyancy sources, such as the crust, the harzburgitic residue, phase changes, and active mantle upwelling, are needed to better understand how shallow slab dynamics is linked to the petrologic and geochemical evolution of the subduction system.
3. Incorporation and testing of more complete rheologies, including non-Newtonian viscosity, low-temperature plasticity, dynamic recystallization (grain-size variations), and lower-mantle (perovskite) flow laws, are needed to determine the fate of slabs in the lower mantle.

DISCLOSURE STATEMENT

The author is not aware of any biases that might be perceived as affecting the objectivity of this review.

LITERATURE CITED

Andrews ER, Billen MI. 2008. Rheologic controls on the dynamics of slab detachment. *Tectonophysics*. In press

Arcay D, Doin MP, Tric E, Bousquet R, de Capitani C. 2006. Overriding plate thinning in subduction zones: localized convection induced by slab dehydration. *Geochem. Geophys. Geosyst.* 7(21–22):Q02007, doi: 10.1029/2005GC001061

Arcay D, Tric E, Doin MP. 2005. Numerical simulations of subduction zones effect of slab dehydration on the mantle wedge dynamics. *Phys. Earth Planet. Inter.* 149:133–53

Becker TW, Faccenna C, O'Connell RJ. 1999. The development of slabs in the upper mantle: insights from numerical and laboratory experiments. *J. Geophys. Res.* 104(B7):15207–26

Bellahsen N, Faccenna C, Funiciello F. 2005. Dynamics of subduction and plate motion in laboratory experiments: insights into the "plate tectonics" behavior of the Earth. *J. Geophys. Res.* 110(B01401), doi: 10.1029/2004JB002999

Benioff H. 1954. Orogenesis and deep crustal structure: additional evidence from seismology. *Bull. Geol. Soc. Am.* 65:385–400

Bevis M. 1988. Seismic slip and down-dip strain rates in Wadati-Benioff zones. *Science* 240:1317–19

Billen MI, Gurnis M. 2001. A low viscosity wedge in subduction zones. *Earth Planet. Sci. Lett.* 193:227–36

Billen MI, Gurnis M. 2003. Comparison of the central Aleutian and Tonga-Kermadec subduction zones: dynamic flow models with a low viscosity wedge. *Geochem. Geophys. Geosyst.* 4(2):1035, doi: 10.1029/2001GC000295

Billen MI, Gurnis M, Simons M. 2003. Multiscale dynamic models of the Tonga-Kermadec subduction zone. *Geophys. J. Int.* 153:359–88

Billen MI, Hirth G. 2004. Rheologic controls on the dynamic evolution of slabs in the upper mantle. *Eos Trans. AGU Fall Meet. Suppl.* 85(47):T23D-03

Billen MI, Hirth G. 2005. Newtonian versus non-Newtonian upper mantle viscosity: implications for subduction initiation. *Geophys. Res. Lett.* 32:L19304, doi: 10.1029/2005GL023457

Billen MI, Hirth G. 2007. Rheologic controls on slab dynamics. *Geochem. Geophys. Geosyst.* 8:Q08012, doi: 10.1029/2007GC001597

Bodri L, Bodri B. 1978. Numerical investigation of tectonic flow in island-arc areas. *Tectonophysics* 50:163–75

Braun MG, Hirth G, Parmentier EM. 2000. The effects of deep damp melting on mantle flow and melt generation beneath mid-ocean ridges. *Earth Planet. Sci. Lett.* 176:339–56

Brudzinski MR, Chen WP. 2000. Variations in P wave speeds and outboard earthquakes: evidence for a petrologic anomaly in the mantle transition zone. *J. Geophys. Res.* 105:21661–82

Cagnioncle AM, Parmentier EM, Elkins-Tanton LT. 2007. The effect of solid flow above a subducting slab on water distribution and melting at convergent plate boundaries. *J. Geophys. Res.* 112:B09402, doi: 10.1029/2007JB004934

Chen WP, Brudzinski MR. 2001. Evidence for a large-scale remnant of subducted lithosphere beneath Fiji. *Science* 292:2475–79

Christensen UR. 1996. The influence of trench migration on slab penetration into the lower mantle. *Earth Planet. Sci. Lett.* 140:27–39

Cížková H, van Hunen J, van den Berg AP. 2007. Stress distribution within subducting slabs and their deformation in the transition zone. *Phys. Earth Planet. Inter.* 161:202–14

Cížková H, van Hunen J, van den Berg AP, Vlaar NJ. 2002. The influence of rheological weakening and yield stress on the interaction of slabs with the 670 km discontinuity. *Earth Planet. Sci. Lett.* 199:447–57

Cloetingh S, Wortel R, Vlaar NJ. 1989. On the initiation of subduction zones. *Pure Appl. Geophys.* 129(1):7–25

Cordier P, Ungár T, Zsoldos L, Tichy G. 2004. Dislocation creep in $MgSiO_3$ perovskite at condition of the Earth's uppermost lower mantle. *Nature* 428:837–40

Däbler R, Yuen DA. 1996. The metastable olivine wedge in fast subduction slabs: constraints from thermo-kinetic coupling. *Earth Planet. Sci. Lett.* 137:109–18

Davies JH, von Blanckenburg F. 1995. Slab breakoff: a model of lithosphere detachment and its test in the magmatism and deformation of collisional orogens. *Earth Planet. Sci. Lett.* 129:85–102

Doin MP, Henry P. 2001. Subduction initiation and continental crust recycling: the roles of rheology and eclogitization. *Tectonophysics* 342:163–91

Dziewonski AM, Anderson DL. 1981. Preliminary reference Earth model. *Phys. Earth Planet. Inter.* 25:297–356

Eberle MA, Grasset O, Sotin C. 2002. A numerical study of the interaction between the mantle wedge, subducting slab, and overriding plate. *Phys. Earth Planet. Inter.* 134:191–202

Elsasser WM. 1968. The Mechanics of continental drift. *Proc. Am. Philos. Soc.* 112(5496):344–53

Enns A, Becker TW, Schmeling H. 2005. The dynamics of subduction and trench migration for viscosity stratification. *Geophys. J. Int.* 160:761–55

Evans B, Fredrich JT, Wong TF. 1990. The brittle-ductile transition in rocks: recent experimental and theoretical progress. In *The Brittle-Ductile Transition in Rocks: The Heard Volume*, ed. AG Duba, WB Durham, JW Handin, HF Wang, Geophys. Monogr. 56, pp. 1–20. Washington, DC: Am. Geophys. Union

Faccenna C, Heuret A, Funiciello F, Lallemand S, Becker TW. 2007. Predicting trench and plate motion from the dynamics of a strong slab. *Earth Planet. Sci. Lett.* 257:29–36

Fei Y, Orman JV, Li J, van Westrenen W, Sanloup C, et al. 2004. Experimentally determined postspinel transformation boundary in Mg_2SiO_4 using MgO as an internal pressure standard and its geophysical implications. *J. Geophys. Res.* 109:B02305, doi: 10.1029/2003JB002562

Ferrari L. 2004. Slab detachment in control on mafic volcanic pulse and mantle heterogeneity in central Mexico. *Geology* 32(1):77–80

Fowler AC. 1993. Boundary layer theory of subduction. *J. Geophys. Res.* 98(B12):21997–2005

Funiciello F, Faccenna C, Giardini D, Regenauer-Lieb K. 2003. Dynamics of retreating slabs: 2. Insights from three-dimensional laboratory experiments. *J. Geophys. Res.* 108(B4):2207, doi: 10.1029/2001JB000896

Funiciello F, Moroni M, Piromallo C, Faccenna C, Cenedese A, Bui HA. 2006. Mapping mantle flow during retreating subduction: laboratory models analyzed by feature tracking. *J. Geophys. Res.* 111:B03402, doi: 10.1029/2005JB003792

Furukawa Y. 1993. Magmatic process under arcs and formation of the volcanic front. *J. Geophys. Res.* 98:8309–19

Garfunkel Z, Anderson CA, Schubert G. 1986. Mantle circulation and the lateral migration of subducted slabs. *J. Geophys. Res.* 91(B7):7205–23

Gerya TV, Yuen DA. 2003. Rayleigh-Taylor instabilities from hydration and melting propel 'cold plumes' at subduction zones. *Earth Planet. Sci. Lett.* 212; doi: 10.1016/S0012-821X(03)00265-6

Gerya TV, Yuen DA, Maresch WV. 2004. Thermomechanical modelling of slab detachment. *Earth Planet. Sci. Lett.* 226:101–16

Goetze C, Evans B. 1979. Stress and temperature in the bending lithosphere as constrained by experimental rock mechanics. *Geophys. J. R. Astron. Soc.* 59:463–78

Green HW, Houston H. 1995. The mechanics of deep earthquakes. *Annu. Rev. Earth Planet. Sci.* 23:169–213

Griffiths RW, Hackney RL, van der Hilst RD. 1995. A laboratory investigation of effects of trench migration on the descent of subducted slabs. *Earth Planet. Sci. Lett.* 133:1–17

Guillou-Frottier L, Buttles J, Olson P. 1995. Laboratory experiments on the structure of subducted lithosphere. *Earth Planet. Sci. Lett.* 133:19–34

Gurnis M, Hager BH. 1988. Controls of the structure of subducted slabs. *Nature* 335(22):317–21

Gurnis M, Hall C, Lavier L. 2004. Evolving force balance during incipient subduction. *Geochem. Geophys. Geosyst.* 5(7), doi: 10.1029/2003GC000681

Hager BH. 1984. Subducted slabs and the geoid: constraints on mantle rheology and flow. *J. Geophys. Res.* 89(B7):6003–15
Hager BH, O'Connell RJ. 1978. Subduction zone backarcs, mobile belts, and orogenic heat. *Tectonophysics* 50:111–33
Hall CE, Gurnis M, Sdrolias M, Lavier L, Müller RD. 2003. Catastrophic initiation of subduction following forced convergence across fracture zones. *Earth Planet. Sci. Lett.* 212:15–30
Han L, Gurnis M. 1999. How valid are dynamic models of subduction and convection when plate motions are prescribed? *Phys. Earth Planet. Inter.* 110:235–46
Hess H. 1962. History of ocean basins. In *Petrological Studies: A Volume in Honor of A. F. Buddington*, ed. EJ Engel, HL James, BF Leonard, pp. 599–620. Boulder, CO: Geol. Soc. Am.
Hirth G. 2003. Laboratory constraints on the rheology of the upper mantle. In *Plastic Deformation of Minerals and Rocks*, ed. SI Karato, HR Wenk, 51:97–116. Washington, DC: Mineral. Soc. Am.
Hirth G, Kohlstedt D. 2003. Rheology of the upper mantle and the mantle wedge: a view from the experimentalists. In *Inside the Subduction Factory*, ed. J Eiler. Washington DC: Am. Geophys. Union
Holmes A. 1944. The Machinery of continental drift: the search for a mechanism. In *Principles of Physical Geology*, pp. 505–9. Edinburgh: Thomas Nelson and Sons, Ltd.
Honda S, Saito M. 2003. Small-scale convection under the back-arc occurring in the low viscosity wedge. *Earth Planet. Sci. Lett.* 216:703–15
Irifune T, Nishiyama N, Kuroda K, Inoue T, Isshiki M, et al. 1998. Postspinel phase boundary in Mg_2SiO_4 determined by in situ X-ray measurement. *Science* 279:1698–700
Isacks B, Molnar P. 1969. Mantle earthquake mechanisms and the sinking of the lithosphere. *Nature* 223:1121–24
Ito E, Takahashi E. 1989. Post-spinel transformations in the system Mg_2SiO_4-Fe_2SiO_4 and some geophysical implications. *J. Geophys. Res.* 94:10637–46
Ji S, Zhao P. 1994. Layered rheological structure of subducting oceanic lithosphere. *Earth Planet. Sci. Lett.* 124:75–94
Karato SI, Riedel MR, Yuen DA. 2001. Rheological structure and deformation of subducted slabs in the mantle transition zone: implications for mantle circulation and deep earthquakes. *Phys. Earth Planet. Inter.* 127:83–108
Katsura T, Yamada H, Shinmei T, Kubo A, Ono S, et al. 2003. Post-spinel transition in Mg_2SiO_4 determined by high p-t in-situ X-ray diffractometry. *Phys. Earth Planet. Inter.* 136:11–24
Katsura T, Ito E. 1989. The system Mg_2SiO_4-Fe_2SiO_4 at high pressures and temperatures: precise determinations of stabilities of olivine, modified spinel, and spinel. *J. Geophys. Res.* 94:15663–670
Katsura T, Yamada H, Nishikawa O, Song M, Kuboet A, et al. 2004. Olivine-wadsleyite transition in the system $(Mg,Fe)_2SiO_4$. *J. Geophys. Res.* 109:B02209, doi: 10.1029/2003JB002438
Kemp DV, Stevenson DJ. 1996. A tensile, flexural model of the initiation of subduction. *Geophys. J. Int.* 125:73–94

Kennett BLN, Engdahl ER, Buland R. 1995. Constraints on seismic velocities in the Earth from travel times. *Geophys. J. Int.* 122:108–24

Kincaid C, Griffiths RW. 2004. Variability in flow and temperatures within mantle subduction zones. *Geochem. Geophys. Geosyst.* 5:Q06002, doi: 10.1029/2003GC000666

Kincaid C, Sacks IS. 1997. Thermal and dynamical evolution of the upper mantle in subduction zones. *J. Geophys. Res.* 102:12295–315

King SD. 2001. Subduction zones: observations and geodynamic models. *Phys. Earth Planet. Inter.* 127:9–24

Kirby SH, Durham WB, Stern LA. 1991. Mantle phase changes and deep-earthquake faulting in subducting lithosphere. *Science* 252(5003):216–25

Kneller EA, van Keken PE, Katayama I, Karato S. 2007. Stress, strain and B-type olivine fabric in the fore-arc mantle: sensitivity tests using high-resolution steady-state subduction zone models. *J. Geophys. Res.* 112:B04406, doi: 10.1029/2006JB004544

Lallemand SE, Heuret A, Boutelier D. 2005. On the relationships between slab dip, back-arc stress, upper plate absolute motion and crustal nature in subduction zones. *Geochem. Geophys. Geosyst.* 6(9):Q09006, doi: 10.1029/2005GC000917

Lay T. 1994. The fate of descending slabs. *Annu. Rev. Earth Planet. Sci.* 22:33–61

Lee CTA, Chen WP. 2007. Possible density segregation of subducted oceanic lithosphere along a weak serpentinite layer and implications for compositional stratification of the Earth's mantle. *Earth Planet. Sci. Lett.* 255:357–66

Li L, Liao X, Fu R. 2002. Slab breakoff depth: a slowdown subduction model. *Geophys. Res. Lett.* 29(3):1041–44, doi: 10.1029/2001GL013420

Litasov K, Ohtani E, Sano A, Suzuki A, Funakoshi K. 2005. In situ X-ray diffraction study of postspinel transformation in a peridotite mantle: implications for the 660-km discontinuity. *Earth Planet. Sci. Lett.* 238:311–28

Mainprice D, Tommasi A, Couvy H, Cordier P, Frost DJ. 2005. Pressure sensitivity of olivine slip systems and seismic anisotropy of earth's upper mantle. *Nature* 433:731–33

McKenzie DP. 1969. Speculations on the consequences and causes of plate motions. *Geophys. J. R. Astron. Soc.* 18:1–32

McKenzie DP. 1977. The initiation of trenches: a finite amplitude instability. In *Island Arc, Deep Sea Trenches and Back-Arc Basins*, ed. M Talwani, WC Pitman, Maurice Ewing Ser., Vol. 105. Washington, DC: Am. Geophys. Union

Moresi L, Gurnis M. 1996. Constraints on the lateral strength of slabs from three-dimensional dynamic flow models. *Earth and Planet. Sci. Lett.* 138:15–28

Moresi L, Zhong S, Gurnis M. 1996. The accuracy of finite element solutions of Stokes' flow with strongly varying viscosity. *Earth Planet. Sci. Lett.* 97:83–94

Morishima H, Kato T, Suto M, Ohtnai E, Urakawa S, et al. 1994. The phase boundary between α- and β-Mg_2SiO_4 determined by in situ X-ray observation. *Science* 265:1202–3

Mosenfelder JL, Marton FC, Ross CR II, Kerschhofer L, Rubie DC. 2001. Experimental constraints on the depth of olivine metastability in subducting lithosphere. *Phys. Earth Planet. Inter.* 127:165–80

Mueller S, Phillips RJ. 1991. On the initiation of subduction. *J. Geophys. Res.* 96(B1):651–65
Nishihara Y, Shinmei T, Karato SI. 2006. Grain growth kinetics in wadsleyite: effects of chemical environment. *Phys. Earth Planet. Inter.* 154:30–43
Niu Y, O'Hara MJ, Pearce JA. 2003. Initiation of subduction zones as a consequence of lateral compositional buoyancy contract within the lithosphere: a petrological perspective. *J. Petrol.* 44(5):851–66
Nothard S, Haines J, Jackson J, Holt B. 1996. Distributed deformation in the subducting lithosphere at Tonga. *Geophys. J. Int.* 127:328–38
Olbertz D, Wortel MJR, Hansen U. 1997. Trench migration and subduction zone geometry. *Geophys. Res. Lett.* 240(3):221–24
Plafker G. 1965. Tectonic deformation associated with the 1964 Alaska earthquake. *Science* 148:1675–87
Poli S, Schmidt MW. 2002. Petrology of subducted slabs. *Annu. Rev. Earth Planet. Sci.* 30:207–35
Ranero C, Morgan JP, McIntosh K, Reichert C. 2003. Bending-related faulting and mantle serpentinization at the middle America trench. *Nature* 425:367–73
Regenauer-Lieb K, Yuen DA, Branlund J. 2001. The initiation of subduction: criticality by addition of water. *Science* 294:578–80
Richards MA, Davies GF. 1989. On the separation of relatively buoyant components from subducted lithosphere. *Geophys. Res. Lett.* 16(8):831–34
Riedel MR, Karato SI. 1997. Grain-size evolution in subducted oceanic lithosphere associated with the olivine-spinel transformation and its effects on rheology. *Earth Planet. Sci. Lett.* 148:27–43
Romanowicz B. 2003. Global mantle tomography: progress status in the past 10 years. *Annu. Rev. Earth Planet. Sci.* 31:303–28
Rubie DC. 1984. The olivine → spinel transformation and the rheology of subducting lithosphere. *Nature* 308:505–8
Rubie DC, Ross CR II. 1994. Kinetics of the olivine-spinel transformation in subducting lithosphere: experimental constraints and implications for deep slab processes. *Phys. Earth Planet. Inter.* 86:223–41
Savage MK. 1999. Seismic anisotropy and mantle deformation: What have we learned from shear wave splitting? *Rev. Geophys.* 374(12):65–106
Schellart WP. 2004. Kinematics of subduction and subduction-induced flow in the upper mantle. *J. Geophys. Res.* 109(B07401):1–19
Schellart WP. 2005. Influence of the subducting plate velocity on the geometry of the slab and migration of the subduction hinge. *Earth Planet. Sci. Lett.* 231:197–219
Schellart WP, Freeman J, Stegman DR, Moresi L, May D. 2007. Evolution and diversity of subduction zones controlled by slab width. *Nature* 446:308–11
Schmeling H, Monz R, Rubie DC. 1999. The influence of olivine metastability on the dynamics of subduction. *Earth Planet. Sci. Lett.* 165:55–66
Sdrolia M, Müller RD. 2006. Controls on back-arc basin formation. *Geochem. Geophys. Geosyst.* 7(4):Q04016, doi: 10.1029/2005GC001090
Stegman DR, Freeman J, Schellart WP, Moresi L, May D. 2006. Influence of trench width on subduction hinge retreat rates in 3-D models of slab rollback. *Geochem. Geophys. Geosyst.* 7(3):Q03012, doi: 10.1029/2005GC001056

Stevenson DJ, Turner JS. 1977. Angle of subduction. *Nature* 270:334–36
Tan E, Gurnis M, Han L. 2002. Slabs in the lower mantle and their modulation of plume formation. *Geochem. Geophys. Geosyst.* 3(11):1067, doi: 10.1029/2001GC00238
Tao WC, O'Connell RJ. 1993. Deformation of a weak subducted slab and variation of seismicity with depth. *Nature* 361:626–28
Tetzlaff M, Schmeling H. 2000. The influence of olivine metastability on deep subduction of oceanic lithosphere. *Phys. Earth Planet. Inter.* 120:29–38
Titus SJ, Medaris LG Jr, Wang HF, Tikoff B. 2007. Continuation of the San Andreas fault system into the upper mantle: evidence from spinel peridotite xenoliths in the Coyote Lake basalt, central California. *Tectonophysics* 429:1–20
Toksöv MN, Minear JW, Julian BR. 1971. Temperature field and geophysical effects of a downgoing slab. *J. Geophys. Res.* 76:1113–38
Toth J, Gurnis M. 1998. Dynamics of subduction initiation at pre-existing fault zones. *J. Geophys. Res.* 103(B8):18053–67
Tovish A, Schubert G, Luyendyk BP. 1978. Mantle flow pressure and the angle of subduction: non-Newtonian corner flows. *J. Geophys. Res.* 83:5892–98
van Hunen J, van den Berg AP, Vlaar NJ. 2001. Latent heat effects of the major mantle phase transitions on low-angle subduction. *Earth Planet. Sci. Lett.* 190:125–35
van Keken PE, Kiefer B, Peacock SM. 2002. High-resolution models of subduction zones: implications for mineral dehydration reactions and the transport of water into the deep mantle. *Geol. Geochem. Geophys.* 3(10):1056, doi:10.1029/2001GC000256
van Wijk JW, Govers R, Furlong KP. 2001. Three-dimensional thermal modeling of the California upper mantle: a slab window vs stalled slab. *Earth Planet. Sci. Lett.* 186:175–86
Vassiliou MS, Hager BH, Raefsky A. 1984. The distribution of earthquakes with depth and stress in subducting slabs. *J. Geodynamics* 1:11–28
Weidner DJ, Wang Y. 1998. Chemical- and Clapeyron-induced buoyancy at the 660 km discontinuity. *J. Geophys. Res.* 103(B4):7431–41
White DA, Roeder DH, Nelson TH, Crowell JC. 1970. Subduction. *Geol. Soc. Am. Bull.* 81:3431–32
Wong A Ton SYM, Wortel MJR. 1997. Slab detachment in continental collision zones: an analysis of controlling parameters. *Geophys. Res. Lett.* 24(16):2095–98
Wortel MJR, Spakman W. 2000. Subduction and slab detachment in the Mediterranean-Carpathian region. *Science* 290:1910–17
Xie S, Tackley PJ. 2004. Evolution of helium and argon isotopes in a convecting mantle. *Phys. Earth Planet. Inter.* 146:417–39
Yamazaki D, Inoue T, Okamoto M, Irifune T. 2005. Grain growth kinetics of ringwoodite and its implication for rheology of the subducting slab. *Earth Planet. Sci. Lett.* 235:871–81
Yoshioka S, Yuen DA, Larsen TB. 1994. Slab weakening: mechanical and thermal-mechanical consequences for slab detachment. *Isl. Arc* 4:89–103
Zeck HP. 1996. Betic-Rif orogeny: subduction of Mesozoic Tethys lithosphere under eastward Iberia, slab detachment shortly before 22 Ma, and subsequent uplift and extensional tectonics. *Tectonophysics* 254:1–16

Zhong S, Davies GF. 1999. Effects of plate and slab viscosities on the geoid. *Earth Planet. Sci. Lett.* 170:487–96

Zhong S, Gurnis M. 1992. Viscous flow model of a subduction zone with a faulted lithosphere: long and short wavelength topography, gravity and geoid. *Geophys. Res. Lett.* 19(18):1891–94

Zhong S, Gurnis M. 1994. Controls on trench topography from dynamic models of subducted slabs. *J. Geophys. Res.* 99(B8):15683–95

Zhong S, Gurnis M. 1995. Mantle convection with plates and mobile, faulted plate margins. *Science* 267:838–43

Annual Review
of Earth and
Planetary Sciences
Volume 36, 2008

Contents

Indexes

Errata

An online log of corrections to *Annual Review of Earth and Planetary Sciences* articles may be found at http://earth.annualreviews.org